Article 25fa pilot End User Agreement

This publication is distributed under the terms of Article 25fa of the Dutch Copyright Act (Auteurswet) with explicit consent by the author. Dutch law entitles the maker of a short scientific work funded either wholly or partially by Dutch public funds to make that work publicly available for no consideration following a reasonable period of time after the work was first published, provided that clear reference is made to the source of the first publication of the work.

This publication is distributed under The Association of Universities in the Netherlands (VSNU) 'Article 25fa implementation' pilot project. In this pilot research outputs of researchers employed by Dutch Universities that comply with the legal requirements of Article 25fa of the Dutch Copyright Act are distributed online and free of cost or other barriers in institutional repositories. Research outputs are distributed six months after their first online publication in the original published version and with proper attribution to the source of the original publication.

You are permitted to download and use the publication for personal purposes. All rights remain with the author(s) and/or copyrights owner(s) of this work. Any use of the publication other than authorised under this licence or copyright law is prohibited.

If you believe that digital publication of certain material infringes any of your rights or (privacy) interests, please let the Library know, stating your reasons. In case of a legitimate complaint, the Library will make the material inaccessible and/or remove it from the website. Please contact the Library through email: copyright@ubn.ru.nl, or send a letter to:

University Library
Radboud University
Copyright Information Point
PO Box 9100
6500 HA Nijmegen

You will be contacted as soon as possible.

1.5-T multiparametric MRI using PI-RADS: a region by region analysis to localize the index-tumor of prostate cancer in patients undergoing prostatectomy

Lars A Reisæter[1,2], Jurgen J Fütterer[3], Ole J Halvorsen[2,4], Yngve Nygård[5], Martin Biermann[1,2], Erling Andersen[6], Karsten Gravdal[4], Svein Haukaas[2,5], Jan A Monssen[1], Henkjan J Huisman[3], Lars A Akslen[2], Christian Beisland[2,5] and Jarle Rørvik[1,2]

Abstract

Background: The use of multiparametric magnetic resonance imaging (mpMRI) to detect and localize prostate cancer has increased in recent years. In 2010, the European Society of Urogenital Radiology (ESUR) published guidelines for mpMRI and introduced the Prostate Imaging Reporting and Data System (PI-RADS) for scoring the different parameters.

Purpose: To evaluate the reliability and diagnostic performance of endorectal 1.5-T mpMRI using the PI-RADS to localize the index tumor of prostate cancer in patients undergoing prostatectomy.

Material and Methods: This institutional review board IRB-approved, retrospective study included 63 patients (mean age, 60.7 years, median PSA, 8.0). Three observers read mpMRI parameters (T2W, DWI, and DCE) using the PI-RADS, which were compared with the results from whole-mount histopathology that analyzed 27 regions of interest. Inter-observer agreement was calculated as well as sensitivity, specificity, positive predictive value (PPV), and negative predicted value (NPV) by dichotomizing the PI-RADS criteria scores ≥ 3. A receiver-operating curve (ROC) analysis was performed for the different MR parameters and overall score.

Results: Inter-observer agreement on the overall score was 0.41. The overall score in the peripheral zone achieved sensitivities of 0.41, 0.60, and 0.55 with an NPV of 0.80, 0.84, and 0.83, and in the transitional zone, sensitivities of 0.26, 0.15, and 0.19 with an NPV of 0.92, 0.91, and 0.92 for Observers 1, 2, and 3, respectively. The ROC analysis showed a significantly increased area under the curve (AUC) for the overall score when compared to T2W alone for two of the three observers.

Conclusion: 1.5 T mpMRI using the PI-RADS to localize the index tumor achieved moderate reliability and diagnostic performance.

[1]Department of Radiology, Haukeland University Hospital, Bergen Norway
[2]Department of Clinical Medicine, University of Bergen, Norway
[3]Department of Radiology, Radboud University Nijmegen Medical Centre, Nijmegen, The Netherlands
[4]Department of Pathology, Haukeland University Hospital, Bergen Norway
[5]Department of Urology, Haukeland University Hospital, Bergen Norway
[6]Department of Clinical Engineering, Haukeland University Hospital, Bergen Norway

Corresponding author:
Lars A Reisæter, Department of Radiology, Haukeland University Hospital, N-5021 Bergen, Norway.
Email: lars.reisaeter@helse-bergen.no

Introduction

Prostate cancer (PCa) is a significant health problem; with an estimated 417,000 new cases in 2012, it is the most common new cancer (23%) in men in Europe (1). Radical prostatectomy and radiotherapy are currently the recommended whole-gland treatments for organ-confined PCa (2), but active surveillance and focal therapies, such as cryosurgery and high-intensity focused ultrasound (HIFU), are also used.

Over the last decade, different methods have been introduced for the detection, localization, characterization, and staging of PCa (3–6). Use of standard morphologic T2-weighted (T2W) magnetic resonance imaging (MRI) rather than clinicopathological characteristics and nomograms in the work-up of PCa has improved local staging (7,8). Several studies support the important finding that most patients have an index tumor responsible for prognosis and outcome (9,10). However, the concept and definition of index tumor is not accepted by all urologists. The definition of index tumor varies to some degree also between pathologists, but an initiative was taken by the International Society of Urological Pathology (ISUP) to agree upon a definition, i.e. the ISUP consensus conference (11).

The use of functional imaging techniques in multiparametric MRI (mpMRI), such as diffusion-weighted imaging (DWI), dynamic contrast-enhanced MRI (DCE), and magnetic resonance spectroscopy imaging (MRSI), have further improved diagnostic performance (12).

Studies on mpMRI of the prostate performed in expert centers have revealed encouraging diagnostic performance (6,13–16), leading to increased use of MRI. The variety in both imaging protocols and diagnostic criteria has made the comparison of results and clinical utility difficult. To reach a consensus on the standardization of protocols and interpretation, the European Society of Urogenital Radiologists (ESUR) published guidelines for prostate imaging protocols and the interpretation of mpMRI, and introduced the Prostate Imaging Reporting and Data System (PI-RADS) as a new scoring system (17). PI-RADS scoring uses specific diagnostic criteria and scores are in the range of 1–5 for each MRI parameter (T2W, DWI, DCE, MRSI, and overall score) (17,18).

The multifocal nature of PCa is a challenge for biopsy procedures, focal therapy, and treatment decisions.

The aim of our study was to evaluate and compare the reliability and diagnostic performance of individual and combined PI-RADS parameters from endorectal 1.5-T mpMRI, using PI-RADS, to localize the index tumor of prostate cancer in patients undergoing robotic-assisted laparoscopic prostatectomy (RALP).

Material and Methods

Patients

In 2010, a total of 72 consecutive patients with biopsy-proven PCa underwent an endorectal 1.5-T mpMRI prior to RALP at our hospital. A retrospective study was performed from which patients were excluded if they had pathologically insignificant tumors according to Epstein criteria (19) (size $\leq$10 mm with a Gleason score of $\leq$3+3) or if the data were incomplete, as shown in Fig. 1. The study was approved by the Regional Committee for Medical and Health Research Ethics, and all patients gave their written consent.

MRI protocol

With patients in the supine position, MRIs were acquired using a 1.5-T whole-body MRI unit (Avanto; Siemens Medical Systems, Erlangen, Germany), using an integrated endorectal and pelvic phased-array coil (MR Innerva; Medrad, Pittsburgh, PA, USA) for signal reception. The endorectal coil was inserted and inflated with a volume of approximately 40–50 mL bariumsulfate (Mixobar®, Bracco Imaging SpA, Milan, Italy). All patients were injected twice with 2 mL betylscopolamin 20 mg/mL (Buscopan; Boehringer Ingelheim GmbH, Ingelheim am Rhein, Germany), both prior to the examination and prior to the DCE, in order to suppress bowel peristalsis.

All images (T2W, DWI, and DCE) covered the entire prostate gland. For contrast enhancement, we used gadoterate meglumin 0.2 mL/kg, (Dotarem®, Guerbet SA, Aulnay-sous-Bois, France). All axial images were obtained using the same positioning angle (center of position and location) as used for the T2W images. For the DWI sequence, we used b values of 50, 400, and 800. In our DCE sequence, the time
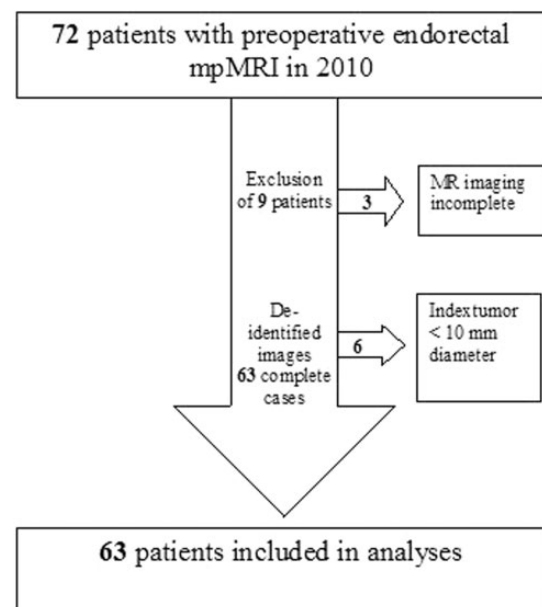

Fig. 1. Inclusion of patients.

resolution was 6.16 s. The scan parameters were consistent for all patients included in the study, with a turbofactor of 16 with the TSE sequence, and all parameters as tabulated in Table 1.

Postprocessing

Calculated, color-coded parametric maps were fused with T2W images using in-house software (20). The software calculates ADC maps from the DWI images and converts the variation in gadolinium concentration, using pharmacokinetic modeling (21,22), into K_{trans}, where the start of enhancement is calibrated using the external iliac artery.

MRI interpretation

Three observers, who all had more than 5 years of experience in reading prostate MRIs, read the MRI datasets independently and in a blind fashion. Observer 1 had more than 5 years' experience in reading mpMRI of the prostate (more than 800 prostate mpMRI examinations), Observer 2 had more than 10 years of experience (more than 2000 mpMRI examinations), while observer 3 had more than 5 years of experience (more than 400 prostate mpMRI examinations). The observers were only informed of biopsy-proven PCa and were blinded to clinical/biochemical results and to the extent of the biopsy findings. To harmonize the use of scoring criteria, the observers performed a pilot study that was not part of this study on 20 patients with histology-proven PCa and mpMRI prior to prostatectomy.

The prostate gland was divided into 27 regions according to the Villers scheme and based on the zonal distribution published by McNeal (23). All regions were individually scored and annotated on separate drawings or directly in the database by the

observers using the PI-RADS. The images of each patient were read sequentially in a single session by the observers in the following order: T2W, DWI, and DCE. Finally, an overall score was given to each separate region based on the information from all sequences.

Histopathology evaluation

Whole-mount, step-section examinations were carried out on the prostatectomy specimens at 5 mm intervals perpendicular to the rectal surface, corresponding to the axial MRI images. Two experienced pathologists (OJH, KG) outlined the presence and extent of each patient's PCa on drawings from the histological sections of the entire prostate. For each specimen, all PCa locations were indicated and a Gleason score was assigned. The presence of a pathologic index tumor was determined by the pathologists using criteria from the ISUP consensus conference, identifying either a single tumor, the tumor with the highest Gleason score (regardless of size), or the tumor with largest volume when multiple tumors with equal Gleason scores were found (11). The volume of the tumors was estimated using routine pathologic measurements (24) and by multiplying the maximum tumor dimensions by height and by 0.52 ($\approx$ volume of a sphere inscribed in a cube). Both pathologists were blinded to MRI findings.

Data analysis

From the histopathology reports and drawings, all index tumors were noted in the corresponding region within the database in consensus by KG and observer 2. In the case of large tumors involving several regions, regions with less than 20% involvement were considered negative for tumor. A true match was defined

Table 1. Imaging protocol; scan parameters of mpMRI.

Sequence	Plane	Repetition time/echo time (msec)	Section thickness (mm)	Intersection gap (mm)	Matrix	Field of view (mm)	Acquisition time
T2W	Sagittal	3030/98	4	0.8	320×256	200×200	3:06 min
T2W	Coronal	3000/98	4	0.4	320×256	200×200	4:05 min
T2W	Axial	4840/84	3	0.8	320×256	200×200	4:18 min
T1 VIBE	Axial	7.23/2.55	3	0.8	192×192	250×250	20 s
DWI (b50, 400, 800)	Axial	3000/72	3	0.8	128×128	128×128	5:33 min
DCE TWIST + C	Axial	4.24/1.66	3	0.8	512×512	192×138	6:58 min

DCE TWIST, dynamic contrast-enhanced time-resolved interleaved stochastic trajectories sequence; DWI, diffusion weighted imaging; iPAT 2, time resolution = 6.16 seconds + C, with intravenous contrast; T1, T1-weighted imaging; T2W, T2-weighted imaging; VIBE, volumetric interpolated breath-hold examination.

by the observer's identification of a focal abnormality on the mpMRI, giving the region a score of ≥ 3, and by histopathology's proving the existence of an index tumor. If the observers/radiologists forgot to score a region, this region was excluded from the statistical analysis.

Statistical analysis

All data were collected using a multidimentional CakePHP application framework (25). A table of prostate regions kept the radiology and the pathology scores for all 27 prostate regions in a separate record for each combination of MR series and observer, and for pathology. Data were re-aggregated using a limited set of SQL views using MySQL (26) and statistical analyses were performed using 'R' (27).

We did not adjust for clustered data. Reliability and diagnostic performance were analyzed separately and in combinations for all the parameters (T2W, DWI, DCE, and overall score) in all regions scored. Interobserver agreement was calculated using the PI-RADS scores from all regions and allowed stratification into peripheral zone regions and transition zone regions.

Patient data were summarized using descriptive statistics by tabulating median values, means, and ranges for continuous variables. Sensitivity, specificity, positive predictive value (PPV), and negative predictive value (NPV) with a 95% CI were calculated. ROC curves were created for the different parameters (T2W, DWI, DCE, and overall score) and further tested for covariance and significance in performance between parameters by comparing the area under the curve (AUC) using bootstrapping with 2000 repetitions.

Cohen's Kappa was used to estimate interobserver agreement between two observers (28), and Light's Kappa (29) was used to estimate inter-observer agreement between all three observers. The 95% CI of Kappa values was calculated based on an exact test of Collett (30) between two observers, and bootstrapping with 1000 repetitions was used when calculating CI between all three observers. All statistical tests were two-sided, and statistical significance was defined on the basis of a P value of less than 0.05 or a Z-score >2.

Results

Patient characteristics are shown in Table 2. A total of 63 patients (with a total of 1701 regions) met the inclusion criteria and were analyzed. Histopathology revealed an index tumor in 365 (21%) of all the 1701 regions, of which 311 (85%) were located in the peripheral zone and 54 (15%) in the transition zone. Furthermore, histopathology demonstrated an index

Table 2. Patient characteristics of patients in our study ($n = 63$).

Age (years)	
Mean	60.7
Median	61.6
Range	(42.9–70.3)
Biopsy – mpMRI (days)	
Mean	130.3
Median	99
Range	(–24–455)
mpMRI operation (days)	
Mean	62.8
Median	70
Range	(1–155)
Index tumor size, maximum diameter (mm)	
Mean	29.1
Median	30
Range	(10–35)
Regions with index tumor	
Index	365
Peripheral zone	311
Transition zone	54
PSA (µg/L)	
Mean	11.6
Median	8.0
Range	(3–81.4)
Index tumor volume (cm³)	
≤ 0.5	8
$0.5 \leq 1.0$	5
$1.0 \leq 2.0$	13
>2.0	37
Index tumor Gleason grade	
3+3	11
3+4	33
3+5	1
4+3	11
4+4	2
4+5	4
5+4	1

tumor in a median of five out of 27 regions per patient (range, 1–19).

The inter-observer agreement by the three observers was 0.41 (Lights Kappa) for overall score and the highest inter-observer agreement for two observers (2/3) of 0.49 (Cohen Kappa), which increased to 0.57 when using the highest score given within any of the

index–tumor regions per patient. The inter-observer agreement was reduced for all three observers in the transition zone when compared to that in the peripheral zone, a reduction which was most prominent between observers 1 and 2 and observers 1 and 3, as shown in Table 3.

Overall score achieved the highest sensitivity of 0.41, 0.60, and 0.55 and NPVs of 0.80, 0.84, and 0.83 in the peripheral zone for observers 1, 2, and 3, respectively. Sensitivity was significantly reduced in the transition zone when compared to the peripheral zone, as shown in Table 4. An example of a characteristic correctly localized index tumor is shown in Fig. 2 (mpMRI) and Fig. 3 (histopathology).

We found significantly improved AUCs in the peripheral zone for overall score (0.64 and 0.72) when compared to T2W (0.59 and 0.68), and improved AUC for DWI (0.62 and 0.72) when compared to T2W (0.59 and 0.68) for observers 1 and 2, respectively. Observers 1 and 3 had a significantly reduced effect of DCE compared to overall score in the peripheral zone. Observers 1 and 2 both had significantly improved AUCs in the peripheral zone for the highest score of any one of the combined parameters (T2W, DWI, or DCE), when compared to the highest score of T2W or DWI. None of the observers had increased AUCs for overall score when compared to any of the highest scores with any combination of the three parameters, T2W, DWI, or DCE, as shown in Table 5 and Fig. 4.

When comparing the differences between observers' AUCs, we found that observer 2 had significantly improved AUCs for all parameters and all combinations of parameters when comparing the AUCs of observer 1. The AUC was significantly improved for DWI and DCE for observer 2 when compared to observer 3. Between observers 1 and 3, the AUC was significantly improved for observer 3 for all parameters except DCE. In the transitions zone there were no significant differences in the AUCs of the three observers for any of the parameters or combinations of parameters. Detection in five of the 63 patients (7.9%), none of the three observers detected the index tumor. The index tumors in these five patients were all located in the peripheral zone, with between one and five regions involved. Gleason scores for these tumors were all $3+4=7$, with a volume of $0.1–2.1\,cm^3$. In three of these five patients additional significant PCa not representing the index tumor was identified by the observers. An example of such is shown in Fig. 5 (mpMRI) and Fig. 6 (histopathology).

Discussion

The observers achieved a moderate inter-observer agreement of 0.41 for overall score. Some papers have

Table 3. Inter-observer agreement (Cohen and Lights Kappa) with confidence intervals (CI) for localization of index tumor in the peripheral and transition zone by mpMRI using PI-RADS for score ≥3.

	Observer 1/2		Observer 1/3		Observer 2/3		Light's kappa	
	Peripheral	Transition	Peripheral	Transition	Peripheral	Transition	Peripheral	Transition
T2W	0.35 (0.29–0.40)	0.15 (0.01–0.33)	0.36 (0.30–0.42)	0.19 (0.03–0.35)	0.43 (0.37–0.49)	0.29 (0.11–0.44)	0.38 (0.34–0.43)	0.21 (0.10–0.33)
DWI	0.36 (0.30–0.43)	0.28 (0.11–0.43)	0.45 (0.37–0.51)	0.31 (0.12–0.48)	0.45 (0.39–0.51)	0.32 (0.14–0.48)	0.42 (0.37–0.47)	0.30 (0.14–0.44)
DCE	0.30 (0.23–0.36)	0.08 (0.01–0.20)	0.40 (0.33–0.46)	0.13 (0.01–0.26)	0.45 (0.39–0.51)	0.44 (0.23–0.62)	0.38 (0.34–0.43)	0.22 (0.10–0.33)
Overall score	0.32 (0.26–0.38)	0.14 (0.02–0.26)	0.42 (0.36–0.48)	0.21 (0.09–0.35)	0.49 (0.44–0.55)	0.43 (0.26–0.61)	0.41 (0.37–0.46)	0.26 (0.15–0.38)

Table 4. Diagnostic performance for localization of index tumor by mpMRI using PI-RADS for score ≥ 3 in peripheral and transition zones; sensitivity, specificity, PPV, and NPV with confidence intervals (CI).

|		True neg Peri/Tran.*	True pos Peri/Tran.*	False neg Peri/Tran.*	False pos Peri/Tran.*	Sensitivity Peripheral (CI)	Sensitivity Transition (CI)	Specificity Peripheral (CI)	Specificity Transition (CI)	PPV Peripheral (CI)	PPV Transition (CI)	NPV Peripheral (CI)	NPV Transition (CI)
T2W	Observer 1	755/498	84/4	227/50	68/15	0.27 (0.25–0.30)	0.07 (0.07–0.12)	0.92 (0.90–0.94)	0.97 (0.95–0.98)	0.55 (0.47–0.63)	0.21 (0.06–0.46)	0.77 (0.74–0.79)	0.91 (0.88–0.93)
	Observer 2	650/480	154/7	157/46	172/29	0.50 (0.44–0.55)	0.13 (0.05–0.25)	0.79 (0.76–0.82)	0.94 (0.92–0.96)	0.47 (0.42–0.55)	0.19 (0.08–0.36)	0.81 (0.78–0.83)	0.91 (0.89–0.94)
	Observer 3	690/484	150/7	160/29	130/47	0.48 (0.43–0.54)	0.13 (0.05–0.25)	0.84 (0.81–0.87)	0.94 (0.92–0.96)	0.54 (0.48–0.60)	0.19 (0.08–0.36)	0.81 (0.78–0.84)	0.91 (0.88–0.93)
DWI	Observer 1	771/490	101/5	210/49	52/23	0.32 (0.27–0.36)	0.09 (0.03–0.20)	0.94 (0.92–0.95)	0.96 (0.93–0.97)	0.66 (0.58–0.73)	0.18 (0.06–0.37)	0.79 (0.76–0.81)	0.91 (0.88–0.93)
	Observer 2	680/478	174/9	136/45	143/31	0.56 (0.50–0.62)	0.17 (0.08–0.29)	0.83 (0.80–0.85)	0.94 (0.91–0.96)	0.55 (0.49–0.60)	0.22 (0.11–0.38)	0.83 (0.81–0.86)	0.91 (0.88–0.93)
	Observer 3	741/494	127/10	184/44	82/19	0.41 (0.35–0.47)	0.19 (0.09–0.31)	0.90 (0.88–0.92)	0.96 (0.94–0.98)	0.61 (0.54–0.67)	0.34 (0.18–0.54)	0.80 (0.77–0.83)	0.92 (0.89–0.94)
DCE	Observer 1	728/468	105/14	206/40	95/45	0.34 (0.29–0.39)	0.26 (0.15–0.40)	0.88 (0.86–0.91)	0.91 (0.88–0.94)	0.52 (0.45–0.60)	0.24 (0.14–0.37)	0.78 (0.75–0.81)	0.92 (0.89–0.94)
	Observer 2	685/495	158/7	152/46	137/15	0.51 (0.45–0.57)	0.13 (0.05–0.25)	0.83 (0.81–0.86)	0.97 (0.95–0.98)	0.54 (0.48–0.59)	0.32 (0.14–0.55)	0.82 (0.79–0.84)	0.91 (0.89–0.94)
	Observer 3	717/493	129/8	182/46	105/20	0.41 (0.36–0.47)	0.15 (0.07–0.27)	0.87 (0.85–0.89)	0.96 (0.94–0.98)	0.55 (0.49–0.62)	0.29 (0.13–0.49)	0.80 (0.77–0.82)	0.91 (0.89–0.94)
Overall	Observer 1	720/470	126/14	185/40	103/43	0.41 (0.35–0.46)	0.26 (0.15–0.40)	0.87 (0.85–0.90)	0.92 (0.89–0.94)	0.55 (0.48–0.62)	0.25 (0.14–0.38)	0.80 (0.77–0.82)	0.92 (0.89–0.94)
	Observer 2	657/486	188/8	123/46	166/25	0.60 (0.55–0.66)	0.15 (0.07–0.27)	0.80 (0.77–0.83)	0.95 (0.93–0.97)	0.53 (0.48–0.58)	0.24 (0.11–0.42)	0.84 (0.81–0.87)	0.91 (0.89–0.94)
	Observer 3	672/482	171/10	140/44	151/30	0.55 (0.49–0.61)	0.19 (0.09–0.31)	0.82 (0.79–0.84)	0.94 (0.92–0.96)	0.53 (0.47–0.59)	0.25 (0.13–0.41)	0.83 (0.80–0.85)	0.92 (0.89–0.94)
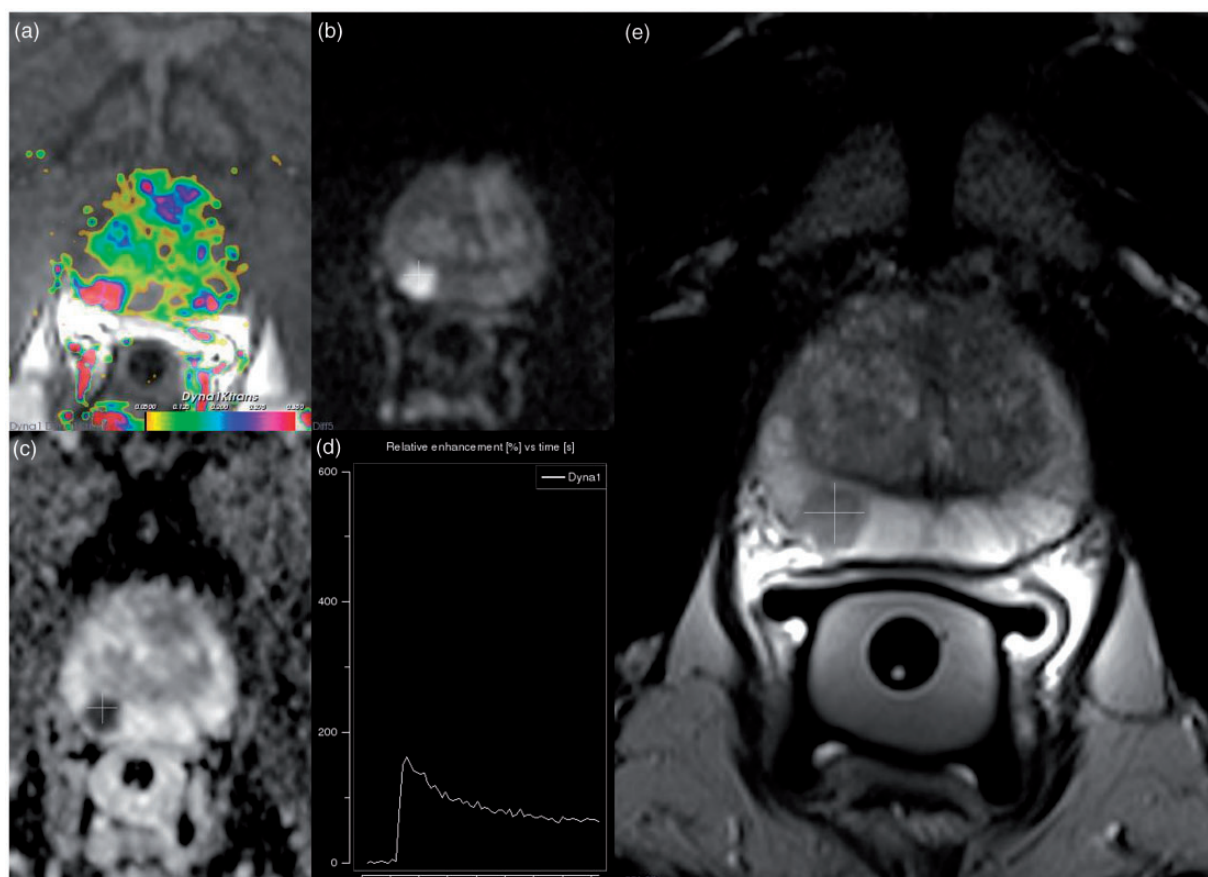
Fig. 2. Multiparametric MRI (mpMRI) of a typical index tumor that was correctly localized. (a) DCE Ktrans parametric map: focal and asymmetric enhancement of a tumor in the right side of the peripheral zone. (b) DWI with b value 800: the tumor shows a high signal in the right side of the peripheral zone. (c) ADC map: the tumor shows low values in the right side of the peripheral zone. (d) Perfusion curve: the tumor shows a typical type-3 curve, fast enhancement, and wash-out. (e) T2W images: the tumor is sharply defined with low signal intensity in the right side of the peripheral zone.
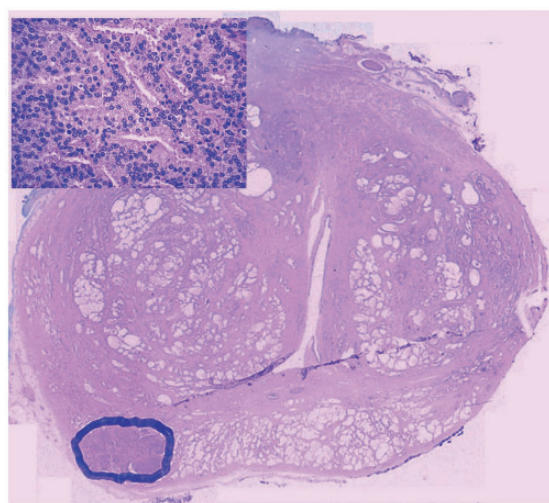

Fig. 3. Whole-mount histopathology from a typical index tumor, shown in Fig. 2. Hematoxylin-Eosin (HE) stain; densely growing tumor in the right side of the peripheral zone; Gleason grade 4 + 4, score 8 (inset magnification ×40).

been published with higher inter-observer agreement in mpMRI used to localize PCa (31,32). The latest report showing inter-observer agreement when comparing the Likert scale with PI-RADS used 16 regions and estimated inter-observer agreement by concordance correlation coefficients rather than kappa coefficients (33). All but the studies of Turkbey et al. and Bratan et al. have fewer regions than our study, and achieve a higher inter-observer agreement (16,34).

The inter-observer agreement was particularly reduced for DCE in the transition zone when compared to the peripheral zone, and this difference was most prominent between observer 1 and the other two observers. One reason for this reduced inter-observer agreement in the transition zone was the low prevalence of index tumors here and the PI-RADS criteria "focal enhancement in an unusual place" may be difficult to anticipate, especially in the transition zone. With more experience/training of the radiologists in the use of PI-RADS in a wide spectrum of cases, the inter-observer agreement may have improved.

Table 5. Area under the curve (AUC) with confidence intervals (CI) in ROC analyses of three observers for the different parameters (T2W, DWI, DCE) and the highest score of either T2W or DWI, T2W or DCE, or T2W, DWI, or DCE and overall score.

		All regions		Peripheral zone		Transition zone	
		AUC	*CI*	*AUC*	*CI*	*AUC*	*CI*
T2W	All observers	0.65	0.63–0.66	0.65	0.63–0.67	0.54	0.51–0.57
	Observer 1	0.59	0.56–0.61	0.59	0.56–0.61	0.52	0.49–0.56
	Observer 2	0.68	0.65–0.71	0.68	0.64–0.71	0.54	0.48–0.59
	Observer 3	0.67	0.65–0.70	0.68	0.65–0.71	0.52	0.48–0.56
DWI	All observers	0.67	0.65–0.68	0.65	0.63–0.67	0.56	0.53–0.59
	Observer 1	0.62	0.60–0.65	0.63	0.61–0.66	0.52	0.48–0.56
	Observer 2	0.72	0.69–0.75	0.73	0.69–0.76	0.55	0.49–0.61
	Observer 3	0.67	0.64–0.69	0.68	0.64–0.70	0.57	0.52–0.62
DCE	All observers	0.65	0.64–0.67	0.65	0.63–0.67	0.59	0.56–0.63
	Observer 1	0.61	0.59–0.64	0.61	0.59–0.64	0.57	0.51–0.63
	Observer 2	0.70	0.67–0.73	0.70	0.67–0.73	0.58	0.52–0.64
	Observer 3	0.65	0.62–0.68	0.65	0.61–0.68	0.58	0.52–0.64
Highest score of either T2W or DWI	Observer 1	0.63	0.61–0.66	0.64	0.61–0.67	0.53	0.48–0.57
	Observer 2	0.72	0.70–0.75	0.73	0.69–0.76	0.57	0.50–0.64
	Observer 3	0.70	0.67–0.72	0.70	0.67–0.73	0.57	0.51–0.63
Highest score of either T2W or DCE	Observer 1	0.63	0.60–0.66	0.63	0.60–0.66	0.58	0.52–0.65
	Observer 2	0.73	0.70–0.76	0.73	0.70–0.77	0.57	0.51–0.64
	Observer 3	0.70	0.67–0.73	0.69	0.66–0.73	0.58	0.52–0.64
Highest score of either T2W, DWI, or DCE	Observer 1	0.65	0.62–0.68	0.65	0.62–0.68	0.57	0.51–0.63
	Observer 2	0.74	0.71–0.77	0.73	0.70–0.77	0.57	0.50–0.64
	Observer 3	0.70	0.67–0.73	0.70	0.66–0.73	0.58	0.52–0.65
Overall score	All observers	0.69	0-67–0.70	0.69	0.67–0.71	0.59	0.55–0.62
	Observer 1	0.64	0.61–0.67	0.65	0.62–0.68	0.57	0.51–0.63
	Observer 2	0.72	0.69–0.75	0.73	0.69–0.76	0.53	0.48–0.59
	Observer 3	0.69	0.67–0.72	0.70	0.67–0.73	0.57	0.51–0.63

The overall score assigned by the observers was compared with three combinations in each region: the highest score of either T2W or DWI, the highest score of either T2W or DCE, or the highest score of one of the three parameters, T2W, DWI, or DCE. We found no significant differences in any of these combinations when comparing them to overall score. Our results support the idea that performing both DCE and DWI does not necessarily increase diagnostic performance regarding localization of the index tumor. We underestimated the extent of the index-tumor regions by only localizing approximately 50% of the tumor, and this is in accordance with the results of previous studies (3,35). Interestingly, almost 90% of all PCa localized by mpMRI comprised index tumors, which is in accordance with previous studies that used a variable number of regions (36,37) and indicates that mpMRI does not increase the identification of insignificant PCa. A diagnostic test with AUCs of 0.65, 0.73, and 0.70, as we achieved, is not perfect, but it might be beneficial for

IMRT-purposes and for urologists making decisions regarding nerve-sparing surgery.

Our study design focused on index-tumor regions, and some of the false-positive regions indeed contained significant PCa not representing index-tumor, which lead to a lower specificity than studies reporting on all PCa tumors. We achieved lower diagnostic performance compared to previously reported studies with consensus readings or studies that took a lesion-by-lesion approach with fewer regions (4–6,14,15,38). The reasons for our lower diagnostic performance could be: (i) the use of a stringent analysis; (ii) the use of a higher number of regions; (iii) that we had no consensus readings between radiologists or between radiologists and pathologists; or (iv) a mixture of these possible reasons. Our diagnostic performance was in concordance with the "neighboring approach" in the study by Turkbey et al. (16) and comparable to the results from the studies of both Bratan et al. (34) and Rosenkrantz et al. (35). The diagnostic performance in
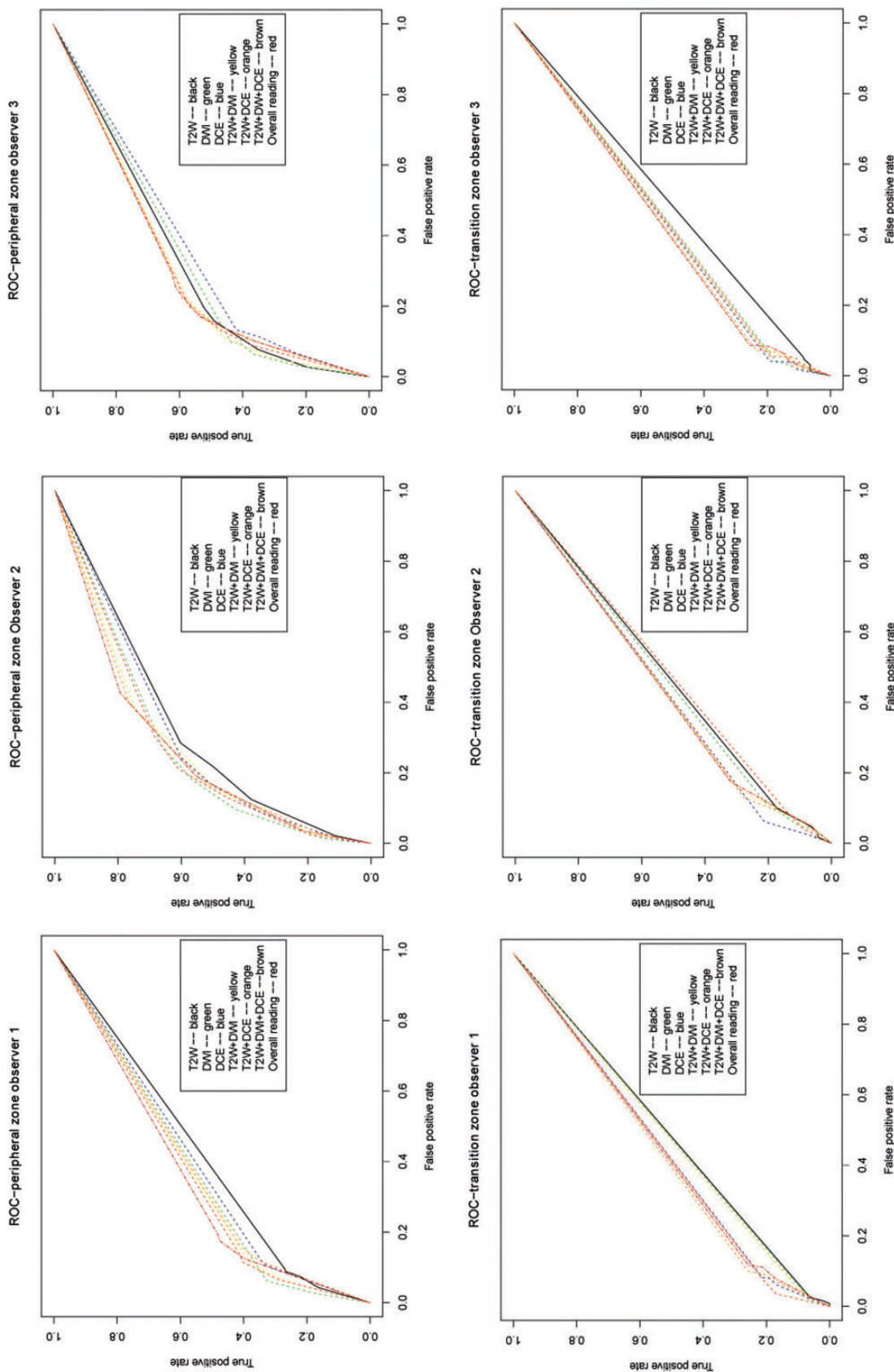
Fig. 4. Individual ROC curves of three observers for localization of index tumor by mpMRI using PI-RADS in the peripheral and transition zone.
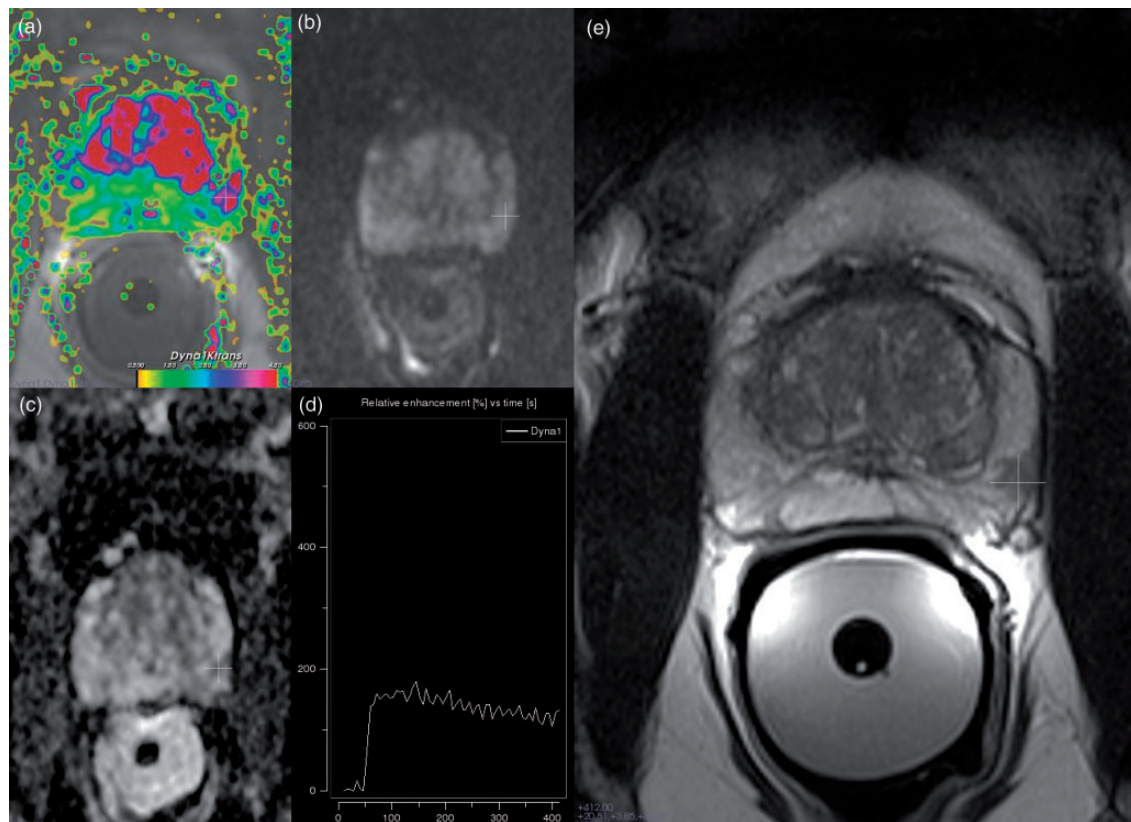
Fig. 5. An undetected index tumor in the right side of the peripheral zone with additional PCa detected with mpMRI in the left side of the peripheral zone. (a) DCE Ktrans parametric map: asymmetric enhancement in the left side of the peripheral zone. (b) DWI with b value 800: no obvious area of high signal intensity. (c) ADC map: a lesion with low signal intensity in the left side of the peripheral zone. (d) Perfusion curve: a lesion with curve type 3; fast enhancement, and wash-out. (e) T2W images: a well-defined lesion with low signal intensity in the left side of the peripheral zone and diffuse lower intensity in the right side of the peripheral zone but no obvious tumor by PI-RADS criteria.
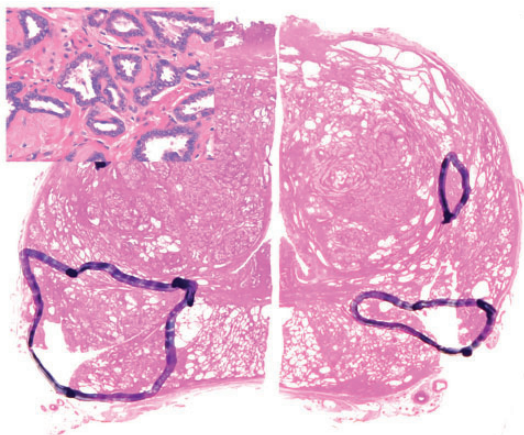

Fig. 6. Whole-mount histopathology (HE-stain) from incorrect index-tumor localization by mpMRI using PI-RADS. Index tumor with scattered glands in greater amount of connective tissue located in the right side of the peripheral zone was not identified. (inset magnification×40); the additional tumor with denser growth in the left peripheral zone was identified by mpMRI; both tumors had Gleason grade 3 + 4, score 7.

the transition zone was lower than that in the retrospective study by Akin (14), and in general, we had a very poor performance in transition zone index tumors. This may be explained by a selection bias as a result of large tumors in the study of Akin and the fact that they used a more lesion-to-lesion–based approach with only 12 regions. Additionally, they did not use DWI and DCE in the study by Akin, but rather relied on T2W images alone.

The variation in diagnostic performances between the observers in our study can be explained by differences in level of experience using Pi-RADS, as well as differences in experience in interpreting mpMRI in general. Our result is not completely supportive of the findings in the study by Vargas et al. (39), in which they found no significantly improved diagnostic performance using T2W images in combination with DWI as compared to the use of T2W images alone. In addition, the index tumors of our study had a higher percentage of Gleason scores $\geq 3 + 4$ than those in the study of Vargas et al. (39), which may also explain the difference in results.

By using the Epstein criteria, we identified four of the six patients with a rather low index–tumor volume of $0.3–0.6\,cm^3$, indicating that PI-RADS has the potential to detect even small index tumors. Some may argue that a shrinkage factor should have been included, but since the Epstein criteria and the consequences of the Epstein criteria are based on pathology and not radiology, we did not adjust for a shrinkage factor. The non-detected index tumors were all localized in the peripheral zone and had limited secondary Gleason grade 4 components. In two of these five patients, the index tumors had a volume of only $0.1\,cm^3$ and $0.2\,cm^3$, respectively, and both were present in one region only. The other three patients had an index tumor located in three to five regions. It is challenging to achieve exact correspondence in location and angle when comparing mpMRI with histopathology whole-mount sections. Further, following prostatectomy, the prostate is deformed due to *ex-vivo* changes in anatomy and histology, resulting both in shrinkage and in mismatches between the pathologic findings and the imaging maps. Turkbey et al. (16) also addressed this problem when evaluating the usefulness of $3\,T$ mpMRI for detecting PCa and found increased sensitivities and specificities for all MRI parameters (T2W, DWI, and MRSI) when using a more tolerant approach. In our study, we used a stringent approach with one-to-one correlation, but regions with less than 20% involvement were considered negative for tumor and achieved almost the same values for diagnostic performance as Turkbey et al. using the tolerant misalignment approach (16). Our proposed 20% criterion for large tumors involving several regions thus seems appropriate.

There are limitations with our study. The differences between the MRI parameters should be interpreted with care, since the parameters in our study were read sequentially and information from one parameter could influence the interpretation of the next parameter. Prostate tumors, including index tumors, are often heterogeneous tumors with different Gleason scores in each of the regions involved. In our analysis, we did not compensate for the differences in Gleason scores between each separate region of the index tumor but instead gave all affected regions an overall pathologic Gleason score. The precision of our PI-RADS scoring is thus not directly correlated to the distribution/heterogeneity of Gleason score findings within the index tumors.

In our analysis, all the radiologists forgot to score some of the regions when reading mpMRI using PI-RADS, resulting in missing data. These missing regions, at most eight regions of 1701 (0.47%), were excluded from the analysis. The numbers of regions that were not annotated by the radiologist yet had an index tumor were at most two of 365 regions (0.55%). The magnitude of our missing data did not alter our conclusion. We did not adjust for clustered data or perform analyses of the different risk groups of patients. In the future, use of $3\,T$ MRI machines, higher temporal resolution ($<4\,s$) in DCE, advances in postprocessing tools, and systematic training of prostate radiologists could improve the diagnostic performance of mpMRI using PI-RADS.

In conclusion $1.5\,T$ mpMRI using the PI-RADS to localize the index tumor achieved moderate reliability and diagnostic performance. Performing both DWI and DCE did not increase diagnostic performance of localization. Almost all index tumors were detected (92%).

Funding

References

1. Ferlay J, Steliarova-Foucher E, Lortet-Tieulent J, et al. Cancer incidence and mortality patterns in Europe: Estimates for 40 countries in 2012. Eur J Cancer 2013; 49:1374–1403.
2. Heidenreich A, Bastian PJ, Bellmunt J, et al. EAU guidelines on prostate cancer. Part 1: screening, diagnosis, and local treatment with curative intent-update 2013. Eur Urol 2014;65:124–137.
3. Zelhof B, Lowry M, Rodrigues G, et al. Description of magnetic resonance imaging-derived enhancement variables in pathologically confirmed prostate cancer and normal peripheral zone regions. BJU Int 2009;104: 621–627.
4. Puech P, Potiron E, Lemaitre L, et al. Dynamic contrast-enhanced-magnetic resonance imaging evaluation of intraprostatic prostate cancer: correlation with radical prostatectomy specimens. Urology 2009;74:1094–1099.
5. Villers A, Puech P, Mouton D, et al. Dynamic contrast enhanced, pelvic phased array magnetic resonance imaging of localized prostate cancer for predicting tumor volume: correlation with radical prostatectomy findings. J Urol 2006;176:2432–2437.
6. Graser A, Heuck A, Sommer B, et al. Per-sextant localization and staging of prostate cancer: correlation of imaging findings with whole-mount step section histopathology. Am J Roentgenol 2007;188:84–90.
7. Wang L, Hricak H, Kattan MW, et al. Prediction of seminal vesicle invasion in prostate cancer: incremental value of adding endorectal MR imaging to the Kattan nomogram. Radiology 2007;242:182–188.
8. Shukla-Dave A, Hricak H, Kattan MW, et al. The utility of magnetic resonance imaging and spectroscopy for predicting insignificant prostate cancer: an initial analysis. BJU Int 2007;99:786–793.
9. Karavitakis M, Winkler M, Abel P, et al. Histological characteristics of the index lesion in whole-mount radical prostatectomy specimens: implications for focal therapy. Prostate Cancer Prostatic Dis 2011;14:46–52.

10. Noguchi M, Stamey TA, McNeal JE, et al. Prognostic factors for multifocal prostate cancer in radical prostatectomy specimens: lack of significance of secondary cancers. J Urol 2003;170:459–463.

11. van der Kwast TH, Amin MB, Billis A, et al. International Society of Urological Pathology (ISUP) Consensus Conference on Handling and Staging of Radical Prostatectomy Specimens. Working group 2: T2 substaging and prostate cancer volume. Mod Pathol 2011;24:16–25.

12. Hoeks CM, Barentsz JO, Hambrock T, et al. Prostate cancer: multiparametric MR imaging for detection, localization, and staging. Radiology 2011;261:46–66.

13. Noworolski SM, Henry RG, Vigneron DB, et al. Dynamic contrast-enhanced MRI in normal and abnormal prostate tissues as defined by biopsy, MRI, and 3D MRSI. Magn Reson Med 2005;53:249–255.

14. Akin O, Sala E, Moskowitz CS, et al. Transition zone prostate cancers: features, detection, localization, and staging at endorectal MR imaging. Radiology 2006;239: 784–792.

15. Futterer JJ, Heijmink SW, Scheenen TW, et al. Prostate cancer localization with dynamic contrast-enhanced MR imaging and proton MR spectroscopic imaging. Radiology 2006;241:449–458.

16. Turkbey B, Pinto PA, Mani H, et al. Prostate cancer: value of multiparametric MR imaging at 3 T for detection–histopathologic correlation. Radiology 2010;255: 89–99.

17. Dickinson L, Ahmed HU, Allen C, et al. Magnetic resonance imaging for the detection, localisation, and characterisation of prostate cancer: recommendations from a European consensus meeting. Eur Urol 2011;59:477–494.

18. Barentsz JO, Richenberg J, Clements R, et al. ESUR prostate MR guidelines 2012. Eur Radiol 2012;22: 746–757.

19. Epstein JI, Walsh PC, Carmichael M, et al. Pathologic and clinical findings to predict tumor extent of nonpalpable (stage T1c) prostate cancer. JAMA 1994;271: 368–374.

20. Vos PC, Hambrock T, Hulsbergen-van de Kaa CA, et al. Computerized analysis of prostate lesions in the peripheral zone using dynamic contrast enhanced MRI. Med Phys 2008;35:888–899.

21. Kovar DA, Lewis M, Karczmar GS. A new method for imaging perfusion and contrast extraction fraction: input functions derived from reference tissues. J Magn Reson Imaging 1998;8:1126–1134.

22. Tofts PS, Brix G, Buckley DL, et al. Estimating kinetic parameters from dynamic contrast-enhanced T(1)-weighted MRI of a diffusable tracer: standardized quantities and symbols. J Magn Reson Imaging 1999;10: 223–232.

23. McNeal JE, Redwine EA, Freiha FS, et al. Zonal distribution of prostatic adenocarcinoma. Correlation with histologic pattern and direction of spread. Am J Surg Pathol 1988;12:897–906.

24. Renshaw AA, Chang H, D'Amico AV. Estimation of tumor volume in radical prostatectomy specimens in routine clinical practice. Am J Clin Pathol 1997;107:704–708.

25. Biermann M. A simple versatile solution for collecting multidimensional clinical data based on the CakePHP web application framework. Comput Methods Programs Biomed 2014;114:70–79.

26. MySQL. 5.2.32 ed2012.

27. R Development Core Team. R: A Language and Environment for Statistical Computing. Vienna Austria, 2012. See http://www.R-project.org/

28. Landis JR, Koch GG. The measurement of observer agreement for categorical data. Biometrics 1977;33: 159–174.

29. Light RJMB. An analysis of variance for categorical data. J Am Stat Ass 1971;66:534.

30. Collett D. Modelling binary data. Boca Raton, FL: Chapman & Hall/CRC; 1999.

31. Schimmoller L, Quentin M, Arsov C, et al. Inter-reader agreement of the ESUR score for prostate MRI using in-bore MRI-guided biopsies as the reference standard. Eur Radiol 2013;23:3185–3190.

32. Rischke HC, Nestle U, Fechter T, et al. 3 Tesla multiparametric MRI for GTV-definition of dominant intraprostatic lesions in patients with prostate cancer–an interobserver variability study. Radiat Oncol 2013;8:183.

33. Rosenkrantz AB, Lim RP, Haghighi M, et al. Comparison of interreader reproducibility of the prostate imaging reporting and data system and likert scales for evaluation of multiparametric prostate MRI. Am J Roentgenol 2013;201:W612–W618.

34. Bratan F, Niaf E, Melodelima C, et al. Influence of imaging and histological factors on prostate cancer detection and localisation on multiparametric MRI: a prospective study. Eur Radiol 2013;23:2019–2029.

35. Rosenkrantz AB, Deng FM, Kim S, et al. Prostate cancer: multiparametric MRI for index lesion localization–a multiple-reader study. Am J Roentgenol 2012; 199:830–837.

36. Nagel KN, Schouten MG, Hambrock T, et al. Differentiation of prostatitis and prostate cancer by using diffusion-weighted MR imaging and MR-guided biopsy at 3 T. Radiology 2013;267:164–172.

37. Hoeks CM, Vos EK, Bomers JG, et al. Diffusion-weighted magnetic resonance imaging in the prostate transition zone: histopathological validation using magnetic resonance-guided biopsy specimens. Invest Radiol 2013;48:693–701.

38. Kim CK, Park BK, Lee HM, et al. Value of diffusion-weighted imaging for the prediction of prostate cancer location at 3T using a phased-array coil: preliminary results. Invest Radiol 2007;42:842–847.

39. Vargas HA, Akin O, Franiel T, et al. Diffusion-weighted endorectal MR imaging at 3 T for prostate cancer: tumor detection and assessment of aggressiveness. Radiology 2011;259:775–784.